Volume 264, Issues 1–2 15 December 2007 ISSN 0012-821X

ELSEVIER

EARTH & PLANETARY SCIENCE LETTERS

Available online at www.sciencedirect.com
ScienceDirect
Earth and Planetary Science Letters 264 (2007) 22–45
EPSL
www.elsevier.com/locate/epsl

Subduction zone evolution and low viscosity wedges and channels

Vlad Manea *, Michael Gurnis

Seismological Laboratory, California Institute of Technology Pasadena, CA 91125, USA

Received 6 December 2006; received in revised form 2 July 2007; accepted 27 August 2007
Available online 14 September 2007
Editor: C.P. Jaupart

Abstract

Dehydration of subducting lithosphere likely transports fluid into the mantle wedge where the viscosity is decreased. Such a decrease in viscosity could form a low viscosity wedge (LVW) or a low viscosity channel (LVC) on top of the subducting slab. Using numerical models, we investigate the influence of low viscosity wedges and channels on subduction zone structure. Slab dip changes substantially with the viscosity reduction within the LVWs and LVCs. For models with or without trench rollback, overthickening of slabs is greatly reduced by LVWs or LVCs. Two divergent evolutionary pathways have been found depending on the maximum depth extent of the LVW and wedge viscosity. Assuming a viscosity contrast of 0.1 with background asthenosphere, models with a LVW that extends down to 400 km depth show a steeply dipping slab, while models with an LVW that extends to much shallower depth, such as 200 km, can produce slabs that are flat lying beneath the overriding plate. There is a narrow range of mantle viscosities that produces flat slabs (5 to10×10^{19} Pa s) and the slab flattening process is enhanced by trench rollback. Slab can be decoupled from the overriding plate with a LVC if the thickness is at least a few 10 s of km, the viscosity reduction is at least a factor of two and the depth extent of the LVC is several hundred km. These models have important implications for the geochemical and spatial evolution of volcanic arcs and the state of stress within the overriding plate. The models explain the poor correlation between traditional geodynamic controls, subducting plate age and convergence rates, on slab dip. We predict that when volcanic arcs change their distance from the trench, they could be preceded by changes in arc chemistry. We predict that there could be a larger volatile input into the wedge when arcs migrate toward the trench and visa-versa. The transition of a subduction zone into the flat-lying regime could be preceded by changes in the volatile budget such that the dehydration front moves to shallower depths. Our flat-slab models shed some light on puzzling flat subduction systems, like in Central Mexico, where there is no deformation within the overriding plate above the flat segment. The lack of in-plane compression in Central Mexico suggests the presence of a low viscosity shear zone above the flat slab.

Keywords: low viscosity; mantle wedge; flat subduction; dip angle

1. Introduction

Dehydration of subducting lithosphere likely transports fluids into the mantle from the slab, affecting the rheology and mechanical coupling to the overriding plate and mantle. There are several sources of fluids in subduction zones, including the subduction of pelagic sediments, previously altered oceanic crust, and serpentinized peridotite below the crust. These fluids, released through dehydration as the mineral assemblages are transformed to higher pressure, migrate upward into the wedge by poorly understood mechanisms (potentially by porous flow, corrosion, hydro-fracturing, buoyant diapirs,

* Corresponding author. Now at: Computational Geodynamics Laboratory, Centro de Geociencias, Campus Juriquilla-Queretaro, UNAM, Mexico.
E-mail addresses: vlad@gps.caltech.edu, vlad@geociencias.unam.mx (V. Manea).

0012-821X/$ - see front matter © 2007 Elsevier B.V. All rights reserved.
doi:10.1016/j.epsl.2007.08.030

or some combination of these). The distribution of dehydration depends on the thermal structure of the subducting slab and mantle wedge, which in turn controls rheology. However, the thermal structure depends on the dip and rate of subduction that maybe controlled by the viscosity of the mantle wedge. In other words, there is likely an intimate balance between dehydration, mantle wedge viscosity, and slab dip.

Rheological laws for peridotite extrapolated to mantle conditions suggest the oceanic asthenosphere should have a low viscosity (10^{18} to 10^{19} Pa s) (Craig and McKenzie, 1986; Karato and Wu, 1993; Hirth and Kohlstedt, 1996). However, regions beneath active volcanic arcs might have viscosities that are even lower than in normal oceanic asthenosphere because of a high fluid flux from the dehydration of subducting slabs. Experiments on the creep of olivine indicate that its viscosity likely decreases exponentially with increasing melt content (Kohlstedt et al., 2000; Mei et al., 2002). The addition of water to upper mantle minerals (olivine) enhances anelasticity and reduces seismic wave velocities. These effects can be quantified through the effects of water on creep that modifies the relaxation time (Karato, 2003). Through water transported from the slab, experiments suggest that the viscosity of the mantle wedge can be up to an order of magnitude lower than normal oceanic asthenosphere (Hirth and Kohlstedt, 2003).

Geophysical observations and models provide valuable constraints on the physical state of mantle wedges. Mantle wedges generally have low seismic velocity and low Q (high attenuation) (Barazangi, and Isacks, 1971; Hasegawa et al., 1991; Roth et al., 2000; Bostock et al., 2002; Abers et al., 2006). For example, the southern Cascadia subduction zone has a low shear velocity zone in the mantle wedge ($\sim -2\%$ perturbation) (Bostock et al., 2002). In the Alaska subduction zone, the mantle wedge has high seismic attenuation where the slab is 80–120 km deep in a region between the slab and continental Moho (Abers et al., 2006). In addition, data from seismic deployments have been analyzed to suggest the presence of low-velocity layers potentially within the top part of the slab. Inland of Cook Inlet in Alaska, dispersion of body waves is consistent with the existence of a thin low-velocity layer (Abers and Sarker, 1996). In the eastern Aleutian subduction zone, anomalous arrivals between P and S have been attributed to a layer with $8\pm2\%$ lower velocity than the overlying mantle, extending to at least 150 km depth (Helffrich and Abers, 1996). From secondary S-wave arrivals for events in the transition zone but recorded on a large array in Japan, Chen et al. (2007) argued for a 20 km thick low-velocity zone on top of the slab that extends down to 300 km. Using, results from five subduction zones, Abers et al. (2006) suggested that low-velocity waveguides maybe common to most subduction zones.

Numerical models of subduction zones consistent with observed seismic structure, topography, geoid and state of stress, require the presence of a low viscosity wedge. Without a low viscosity wedge, dynamic models predict excessively deep back-arc regions, geoid lows, and in-plate compression. A low viscosity zone, with a reduction in viscosity by about an order of magnitude, attenuates the downward force on the overriding plate (Billen and Gurnis, 2001; Billen et al., 2003). Three-dimensional dynamic models of the Tonga–Kermadec and Aleutian subduction zones are only consistent with the geoid if a zone with viscosity at least an order of magnitude lower than the surrounding asthenosphere is included (Billen and Gurnis, 2003).

Slab dip may also provide important constraints on rheology. The geometry of subducted slabs varies from flat (e.g. Mexico, Peru, Chile) to nearly vertical (e.g. Mariana). Beneath Peru, the geometry of the Nazca plate shows a flat-slab segment at $\sim$100 km depth, extending for several hundred km beneath the continent. Beneath central Chile, seismicity delineates a flat slab located at 100–120 km depth, extending horizontally for 500–600 km from the trench (Gutscher et al., 2000). In Central Mexico the flat slab is located at only 40–45 km depth and extends for 250–300 km from the trench (Suarez et al., 1990). Approximately 10% of present day subduction zones may be represented by flat subduction (Gutscher et al., 2000).

Slab dip may be related to a balance between the gravitational body force and slab suction (Tovish et al., 1978; Stevenson and Turner, 1997). This suggests that slab age is an important control on the dip of slabs, but the correlation between slab dip and age is non-existent (Cruciani et al., 2005) or moderate (Jarrard, 1986; Lallemand et al., 2005; Tape et al., in preparation). If traditional geodynamic concepts predict such straightforward correlations between slab dip, age and convergence, why are the observed correlations not more robust? Obviously, there must be aspects of subduction physics that have yet to be adequately understood. With an increasing evidence of significant viscosity variations in the upper mantle above the subducting slabs (Billen and Gurnis, 2001; Hirth and Kohlstedt, 2003), mantle wedge viscosity might be one of the key parameter controlling subduction geometry.

Here, we investigate numerically the effect of low viscosity wedges and channels on the evolution of slab geometry. We investigate slab evolution as a function of wedge and channel viscosity and geometry. Our modeling technique differs from previous dynamic models (van

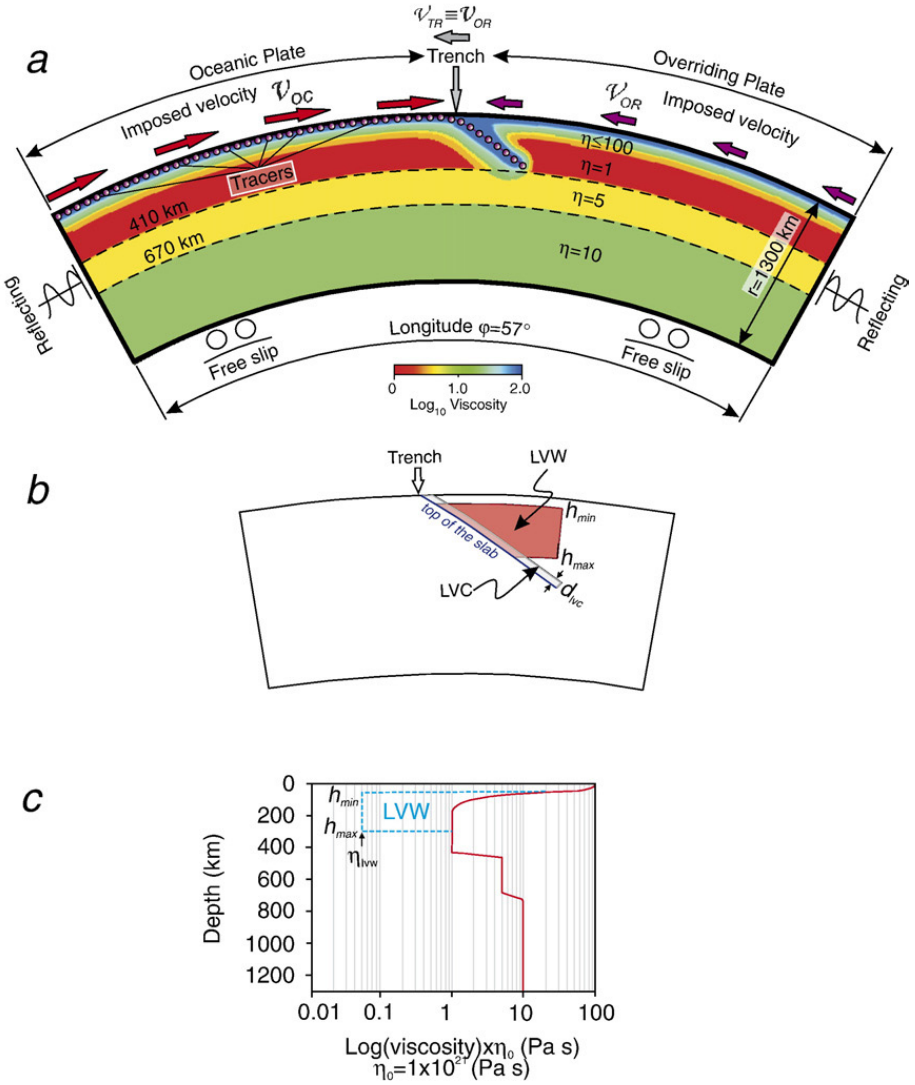

Fig. 1. a. Initial viscosity configuration of 2-D models. There are two tectonic plates on top, the subducting (left) and overriding (right). The velocities of these plates are v_{OC} and v_{OR}. The trench has the same velocity as the overriding plate $v_{TR}=v_{OR}$. b. Initial LVW and LVC geometry and controlling parameters: h_{MIN}, h_{MAX}, and d_{LVC}. The LVW width at h_{MAX} is kept constant at $w=50$ km. c. The non-dimensional viscosity profile.

Hunen, 2001) where the zone of weakness was defined in the form of an *a priori* prescribed fault. Here, we use tracers that simulate the subduction of crust and sediments advected with the flow. With rules, zones of altered viscosity are generated above the slab depending on pressure and distance from the trench. In these models, there is an intimate balance between the low viscosity zones and the evolution of the subduction zone structure, including slab dip.

2. The numerical models

2.1. Basic equations and viscosity formulation

Mantle convection is governed by the coupling between fluid flow and energy transport, while neglecting inertial terms. The calculations are performed in a 2-D cut through a sphere on a non-deforming grid, by solving the conservation equations of mass, momentum and energy while making the Boussinesq approximation.

Table 1
Model parameters held constant

Parameter		Value
Reference density	ρ_0	3300 kg/m^3
Temperature contrast	ΔT	1500 K
Thermal diffusivity	K	1×10^{-6} m^2/s
Thermal expansion	a	2×10^{-5} 1/K
Earth radius	R_0	6371.137 km
Gravitational acceleration	G	10 m/s^2
Reference viscosity	η_0	1×10^{21} Pa s

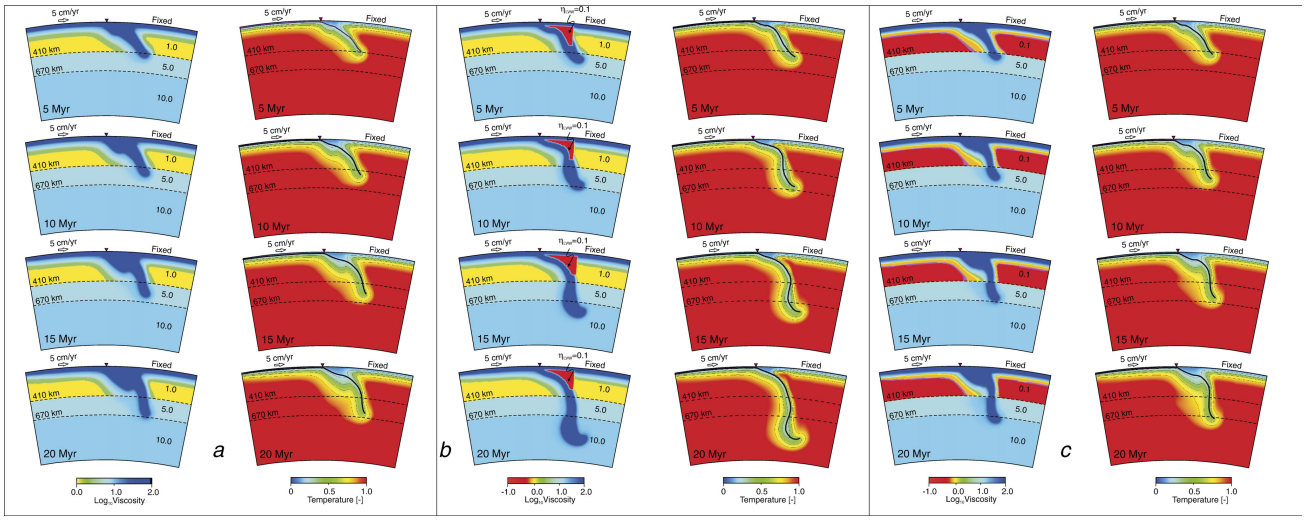

Fig. 2. a. Model evolution with no LVW included. b. The introduction of the LVW (h_{MIN}=40 km, h_{MAX}=300 km, w=50 km, η_{LVW}=0.1). c. Same as the model in (a), except that the upper mantle viscosity is lowered from 10^{21} Pa s to 10^{20} Pa s. All models have a fixed upper plate and the oceanic plate moves at 5 cm/yr.

The equations are written in non-dimensional form and the summation over indices is implicit:

$$\mu_{i,j} = 0 \tag{1}$$

$$-P_{,i} + \left(\eta u_{i,j} + \eta u_{j,i}\right)_{,j} + \mathrm{Ra} T \delta_{\mathrm{ir}} = 0 \tag{2}$$

$$T_{,i} + u_i T_{,i} = T_{,ii} + \gamma \tag{3}$$

Where, u_i is the velocity, P is the dynamic pressure, Ra is the Rayleigh number, η is the viscosity, T is the temperature, and γ is the heat production rate. $X_{,y}$ represents the derivative of X with respect to y, i and j are spatial indices, and t is time. Ra is defined as $Ra = \frac{\rho g \alpha \Delta T R_0^3}{\eta_0 \kappa}$. Where κ is the thermal diffusivity, ΔT is the superadiabatic temperature drop, η_0 is the dimensional reference dynamic viscosity, R_0 is the radius of the Earth, α is the thermal expansivity. The mantle is divided into four layers: lithosphere (0–100 km), upper mantle (100–410 km), transition zone (410–670 km) and part of the lower mantle (670–1300 km). The viscosity is temperature- and depth-dependent:

$$\eta(r,T) = f(r) e^{\left(\frac{c1}{c2+T} - \frac{c1}{c2+T_m}\right)} \tag{4a}$$

$$f(r) = \eta_{\mathrm{LVW}} \text{ and } c1 = 0 \text{ if inside wedge} \tag{4b}$$

where $f(r)$ is a non-dimensional value that differs in each layer. The dimensional viscosity in each layer is obtained by multiplying the non-dimensional value with the reference value, $\eta_0 = 10^{21}$ Pa s. A non-dimensional viscosity variation of 10^4 or 0.01–100 is used across the whole domain. For our nominal set of calculations, the non-dimensional parameters were set to $c1 = 7$ and $c2 = 0.1$ with a viscosity cut-off of 100 and were chosen so that the dimensional viscosity of the slab did not exceed $\sim 10^{23}$ Pa s. Three-D models constrained by observed structure and consistent with topography and gravity show that if slab viscosities exceed 10^{23} Pa s, then strain rates are lower than seismic strain rates (Billen et al., 2003). Since total strain rates must be a sum of seismic and aseismic processes, modeled values must always exceed seismic values to be realistic. However, we also ran models with larger non-dimensional activation energies ($c1$, including 5, 7, 10 and 17.64). With larger $c1$ and cut-off values, we find that slabs transition to a buckling regime. However, we focus on slabs with viscosities of $\sim 10^{23}$ Pa that are consistent with seismic evidence. $T_m = 1$ is the non-dimensional temperature of ambient mantle.

Using the finite element package *CitcomS Version 2.0.1* (Tan et al., 2006) available from the Computational Infrastructure for Geodynamics (CIG) (http://geodynamics.org), the computations are performed within a thin spherical domain (r,ϕ), where r is radius and ϕ is longitude. The inner radius corresponds to a depth of 1300 km, the outer radius the surface of the Earth. The span in longitude is 57°. This domain is evenly divided into 128 elements in the radial and 640 in longitude, corresponding to a 10×10 km resolution. Tests were performed with finer resolution grids. The boundary conditions are as follows. The top and bottom boundaries are isothermal. The top boundary has an imposed velocity boundary condition, the bottom is free slip, and the sides are reflecting. The initial thermal structure is described by a thermal boundary layer (age controlled) at the top and isothermal mantle with an initial slab with a 30° dip angle (Fig. 1a). A typical vertical viscosity profile is presented in Fig. 1c. Parameters held constant are summarized in Table 1.

2.2. Particle tracers and low viscosity wedges and channels

In order to study the influence of low viscosity wedges and channels, we use a tracer method and a parameterized approach. The parameterized approach is used to broadly explore LVW geometry and viscosity on structure; the LVW geometry is a complex multi-physics problem addressed in a companion study (Baker et al., submitted for publication). A set of particle tracers (5,000) is evenly distributed on the top of the oceanic plate at a depth of 5 km and along the initial slab geometry (see Fig. 1a). The tracer spacing, ~ 500 m, is much smaller than the mesh resolution. Tracer velocity is calculated by interpolating the eight nodal velocities with the bilinear shape functions. Tracers are advected with the mid-point method (2nd order accuracy). Low viscosity wedges and channels are generated from the geometry of the subducted crust. We defined three parameters that control the low viscosity wedge: minimum depth (h_{MIN}), maximum depth (h_{MAX}), and wedge viscosity (η_{LVW}). The maximum horizontal extent (w) of the LVW is measured from the slab surface at h_{MAX} (Fig. 1b). We use a constant value of w of 50 km for all LVW models. For the low viscosity channels, we have a channel thickness (d_{LVC}).

2.3. Initial model setup

Model initial conditions were generated in the following way. We placed tracers on top of the oceanic

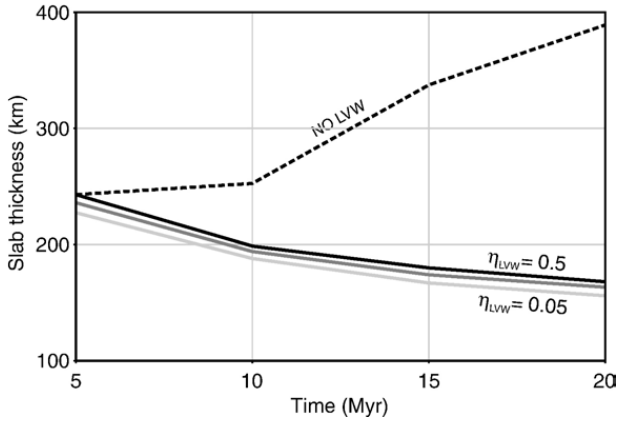

Fig. 3. Slab thickness (defined in terms of the 0.8 isotherm measured at 300 km depth) as a function of time for a model with no LVW and three models with different viscosity reductions within the wedge.

plate for a model with an isothermal mantle. Then, while the tracers are advected, we lower the viscosity (by 0.1) above the tracers with a d_{LVC} of 20 km for depths below 10 km, creating a low viscosity channel that controls slab dip. By integrating plate kinematics forward for 30 Myr a well behaved slab formed that extends down to ~400 km depth (Fig. 1a). The thermal structure and position of the tracers was then used as the initial condition for subsequent calculations.

3. Model results

While the top velocity boundary conditions are held fixed so that there is no trench rollback, we first investigate the influence of low viscosity wedges and channels on the time-space evolution of subduction zone structure, pressure and arc position. Then, we explore the influence of the low viscosity wedges and channels with a constant trench roll back.

3.1. Time-dependent models with low viscosity wedges

We find that the introduction of a low viscosity wedge above the subducting slab has a substantial effect on subduction zone structure, including slab dip. In this first set of calculations, a constant convergence rate of 5 cm/yr, an initial and uniformly thick (50 Ma) lithosphere with no trench migration was assumed. Without an LVW, we reproduce behavior previously found: a shallow dipping

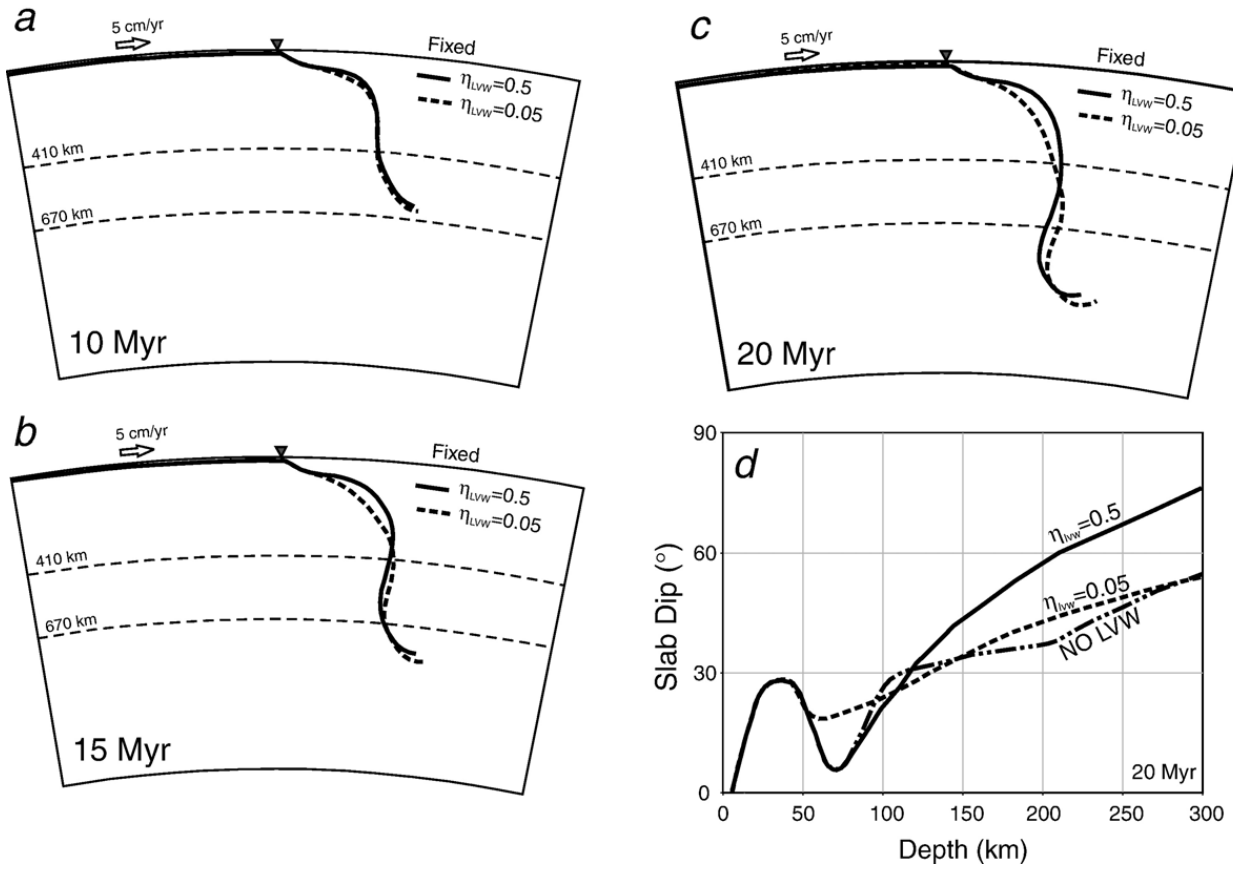

Fig. 4. a–c. Slab shape (denoted with the trace of subducted oceanic crust) as a function of time for two models with η_{LVW}=0.5 and η_{LVW}=0.05 after 10, 15 and 20 Myr of convergence from the initial condition. d. Local slab dip as a function of depth for these two models after 20 Myr of convergence.

slab with substantial advective thickening (the high mantle wedge viscosity causes a barrier to flow) (Olbertz, 1997).

Starting with a ~30° dipping slab with an initial length of ~500 km, after 20 Myr of additional convergence, the trace of oceanic crust rises with substantial advective thickening and a commensurate increase in viscosity above the slab (Fig. 2a). This overall slab behavior is approximately independent of upper mantle viscosity, as shown in Fig. 2c for a case when the entire upper mantle viscosity was lowered from 10^{21} Pa s to 10^{20} Pa s. This structure is qualitatively inconsistent with that determined from seismology, because of the approximate doubling of slab thickness. With the introduction of a LVW (h_{MIN}= 40 km, h_{MAX}=300 km, w=50 km, η_{LVW}=0.1) the subduction structure changed significantly (Fig. 2b). At 5 Myr after the inclusion of the LVW, higher temperature upper mantle penetrates further into the top of the mantle wedge. With the smaller resistance of the slab from the overriding plate, the slab penetrates more deeply into the transition zone compared to the case without a LVW. By 10 Myr, the slab is not advectively thickened within the upper mantle, as it is in the models without an LVW (Fig. 2a). As subduction continues, the differences between the models increase as the slab fully penetrates into the lower mantle. With the introduction of the LVW, the excessive advective thickening is eliminated. Models without LVW show that slab thickness (defined in terms of the 0.8 isotherm at 300 km depth) increases from ~350 km to >400 km (Fig. 3) (initial slab thickness, measured at 300 km depth, is 315 km). With the incorporation of the LVW, more realistic slab thicknesses are obtained and slab thickness decreases with time (i.e. ~160 km after 20 Myr). The first 50% reduction in the wedge viscosity from a uniform upper mantle background viscosity has a large effect on decreasing slab thickness but additional reductions in viscosity reduce the thickness by only small amounts (Fig. 3).

Incorporation of the LVW changes slab dip, as shown for models that have been integrated for 20 Myr (Fig. 4). Although the relation is complex, comparison of models with different viscosity reductions clearly shows the influence of wedge viscosity on slab dip (Fig. 4). Without a substantial reduction in wedge viscosity, the

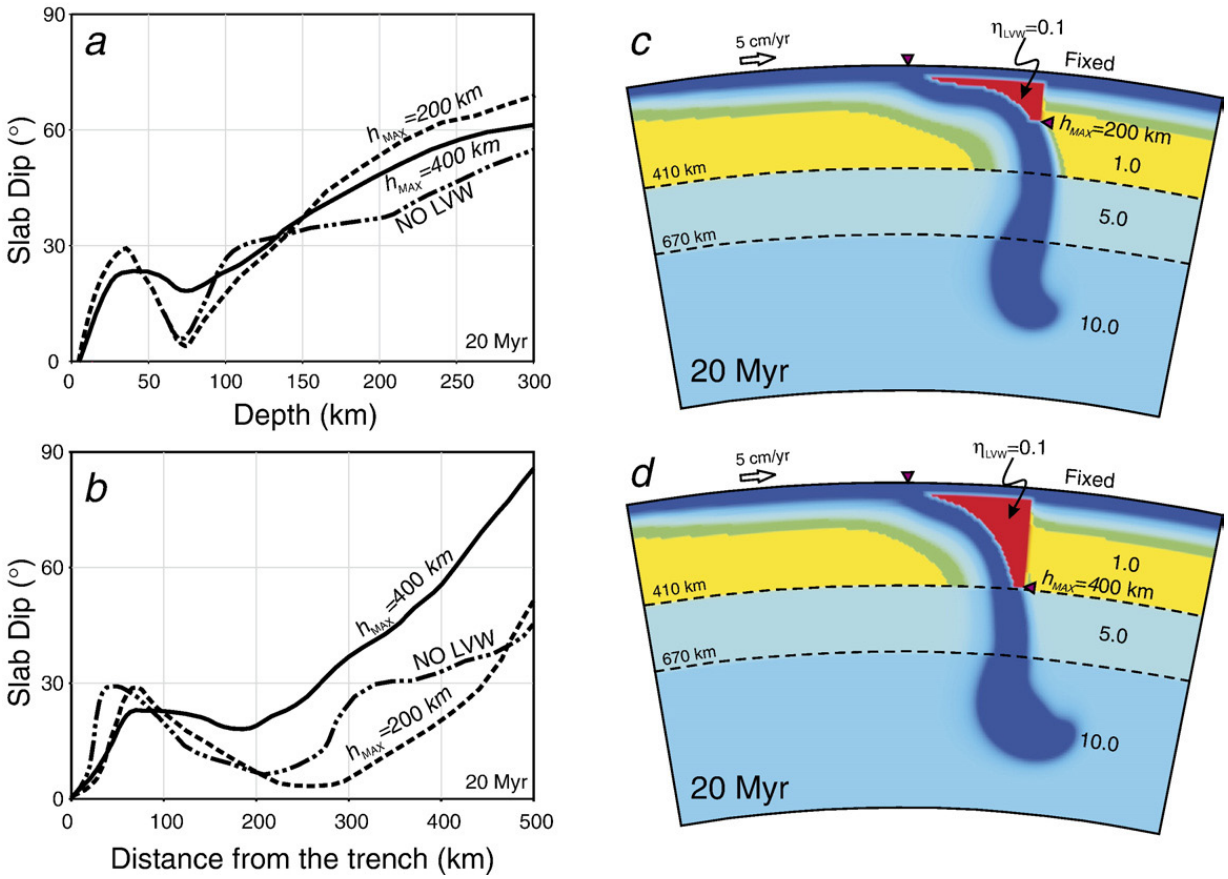

Fig. 5. The influence of the maximum depth of the LVW (h_{MAX}) on slab structure shown in terms of the local slab dip as a function depth (a) and distance from the trench (b) after 20 Myr of convergence. c. Viscosity distribution for the model with the shallow LVW (h_{MAX}=200 km) after 20 Myr. d. Viscosity distribution for the model with the deep LVW (h_{MAX}=400 km) after 20 Myr. In c and d, the non-dimensional viscosity of each layer is shown.

slab remains at a shallower dip for a larger distance from the trench so that when the slab does dip into the upper mantle it does so at a deeper dip. With small viscosity reductions, this leads to an inflexion in slab dip in the depth range 50–100 km (Fig. 4d). A stronger viscosity reduction allows the slab to more gradually change dip at greater depth. The slab dip for models with $\eta_{LVW}=0.5$ continues to show small dip angles (<10°) (Fig. 4d), but lowering the wedge viscosity by even more, 0.05, causes the slab dip to increase to ~20° in the 50–100 km depth range. How the dip changes as a function of time in these two models, $\eta_{LVW}=0.5$ and $\eta_{LVW}=0.05$, is diagnostic (Fig. 4a–c). After 10 Myr of convergence and about 100 km from the trench, the depth of the top of the crust progressively increases when the wedge viscosity decreases.

The maximum depth of the LVW (h_{MAX}) has a strong influence on slab structure and can cause slab dip to change substantially for depths <150 km (Fig. 5). For shallow LVW (200 km) the slab has a small, ~10°, dip within the 50 to 100 km depth range (Fig. 5d). This model shows a ~100 km flat-slab segment located from 200 to 300 km from the trench (Fig. 5b). Increasing the depth extension of the LVW (400 km) gives rise to a steeper slab (Fig. 5d). In other words, when the low viscosity wedge is shallow, it tends to promote flat flying subduction (Fig. 5b). Since, models with no LVW have flat-lying subduction, it appears that LVW can either lead to more extreme flat-lying subduction or eliminate flat-lying subduction entirely depending on the geometry of the viscosity reduction. Even though slab dip is small in both no-LVW cases and shallow-LVW cases (Figs. 2a and 5c, respectively), the slab structure differs considerably between the two. With no LVW, we find both small dips and excessive thickening; while with the shallow LVW, the models have small dips but no excessive thickening. With a shallow LVW, flat-lying subduction is enhanced because viscous resistance between the slab and overriding plate is reduced, allowing the slab to penetrate further beneath the overriding plate.

The pressure distribution provides insight on the relationship between slab dip and the LVW. As shown for two models, $\eta_{LVW}=1.0$ and 0.1 (Fig. 6), although the initial conditions are the same (see Fig. 1), the pressure distribution above the slabs differs considerably after 20 Myr of convergence. With a high wedge viscosity,

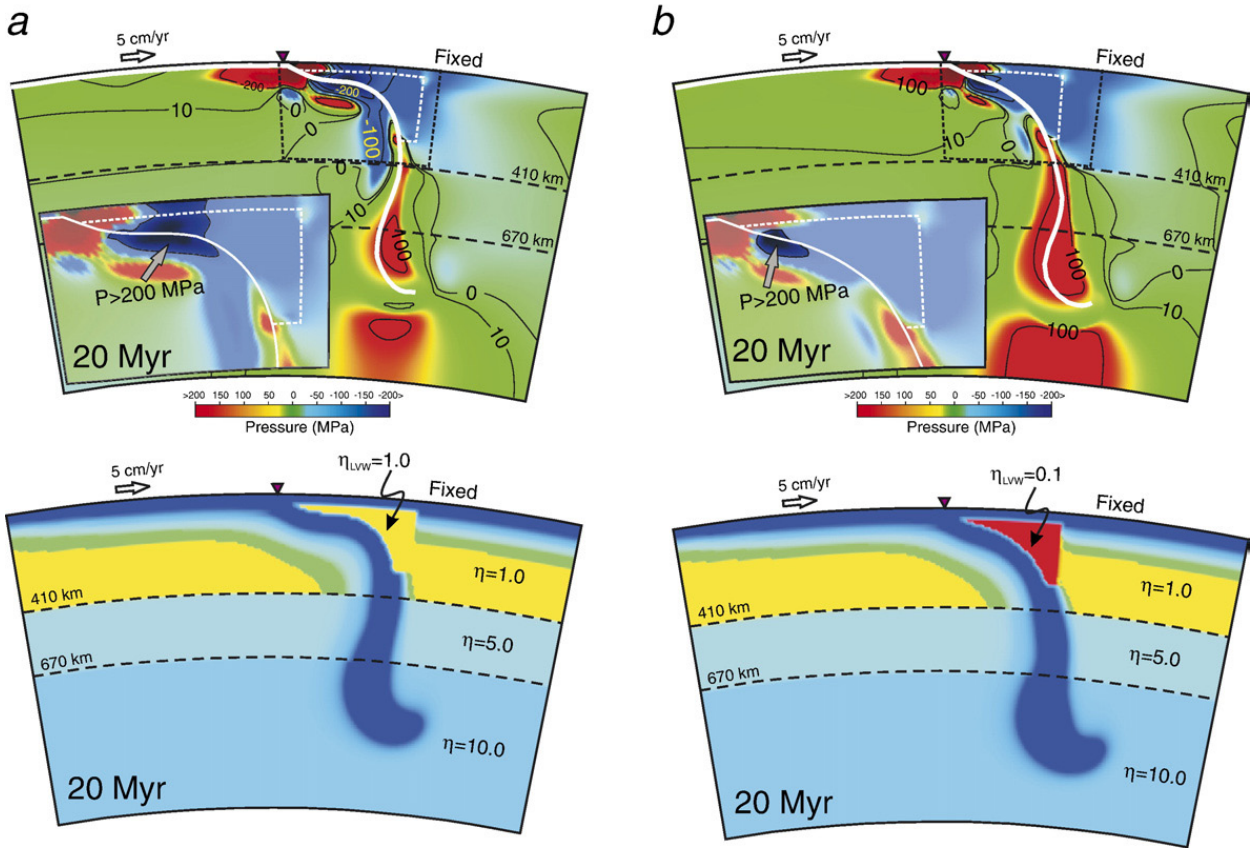

Fig. 6. The pressure distribution (upper) and viscosity (bottom) for models with $\eta_{LVW}=1.0$ (a) and $\eta_{LVW}=0.1$ (b).

there is a region of negative pressure greater than 200 MPa (Fig. 6a, inset), but the size of this region decreases considerably as the scaled mantle wedge viscosity decreases from 10^{21} Pa s to 10^{20} Pa s. The models show a bimodal pressure distribution: positive pressure beneath the subducting slab, and negative pressure above the slab. The high negative pressure for models with high wedge viscosity pulls the slab to shallower depth so that the slab has small dip angles. Models with a LVW reduces the suction force occurring in the depth range between 100 to 300 km depth allowing the slab to more evenly descend into the lower mantle.

A lower viscosity within a localized region is critical for the reduction in the pressure force that allows the slab can fall away from the overriding plate. A reduction in the entire upper mantle viscosity (Fig. 2c) or a reduction in the viscosity of the region above the slab but with a viscosity identical to the rest of the upper mantle (i.e. Fig. 6a) are individually insufficient to allow the slab to freely fall away from the overriding plate. It is only the combination of these two effects (Fig. 6b), which reduces the pressure above the slab as it moves into the upper mantle. We have documented this phenomena and scaled η_0 in the range 10^{19} Pa s to 10^{21} Pa s. Reducing only the upper mantle viscosity does not increase slab dip because there is no decoupling zone between the slab and overriding plates at shallow depths; the slab cannot fall away from the overriding plate without decoupling.

3.2. Time-dependent models with low viscosity channels

As an alternative formulation, we have introduced a low viscosity channel (LVC) on top of the slab. This geometry is motivated by observations in Japan and Alaska described above for narrow low seismic velocity zones above the slabs. In a sense, these channels can be view as either deep “faults” or “shear zones”, although the process for formation may be slab dehydration. As with the LVW, we observed a significant change in the subduction slab structure.

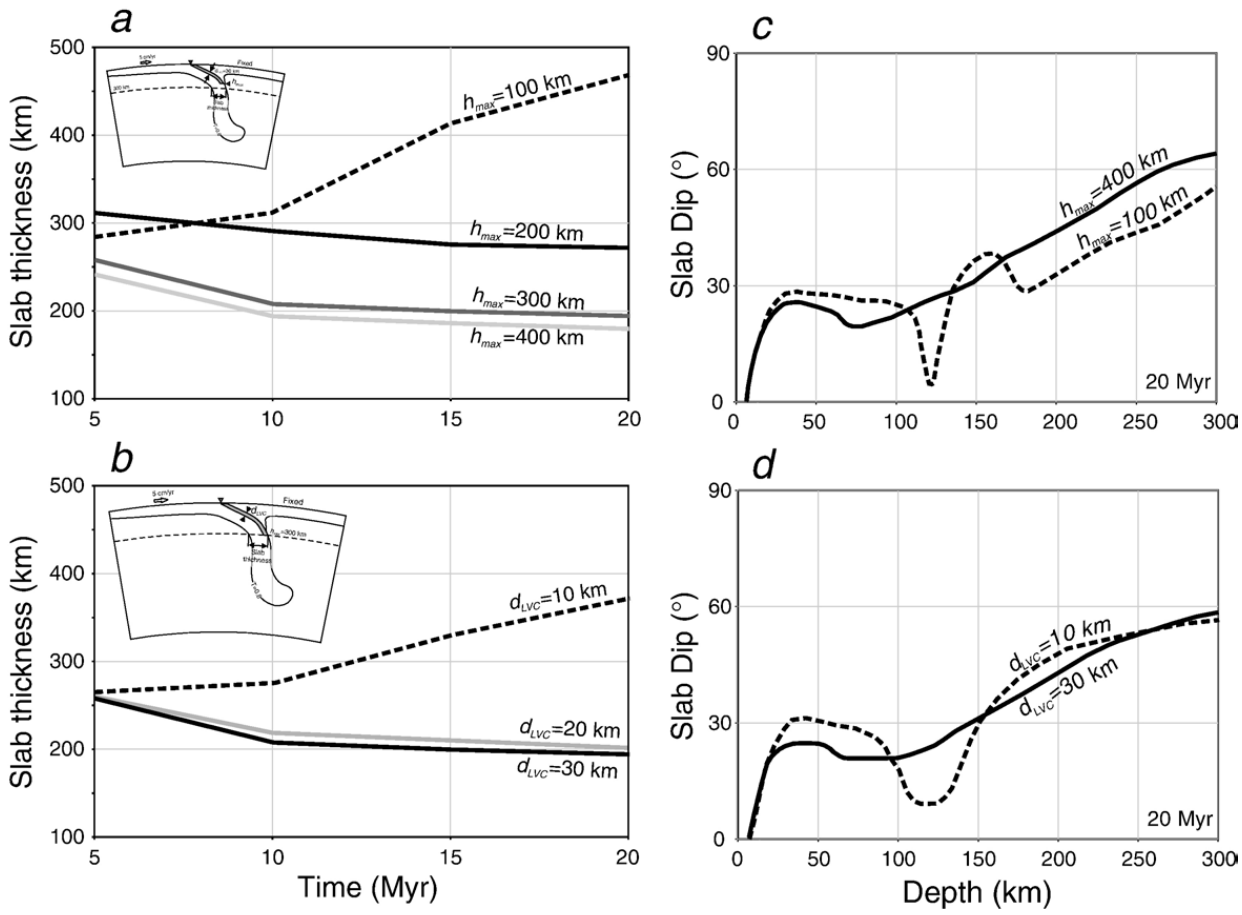

Fig. 7. Evolution of slab thickness and local slab dip as function of depth for LVC models. a. Slab thickness as a function of time for LVC models in which h_{MAX} is varied from 100 to 400 km while thickness of LVC is held at a constant 30 km. b. Slab thickness as function of time for LVC models in which d_{LVC} is varied from 10 to 30 km while the depth is held fixed at 300 km. c. Local slab dip as a function of depth for two models with different maximum LVC depth h_{MAX}=100 and 400 km. d. Local slab dip as a function of depth with different LVC thickness d_{LVC}=10 and 30 km.

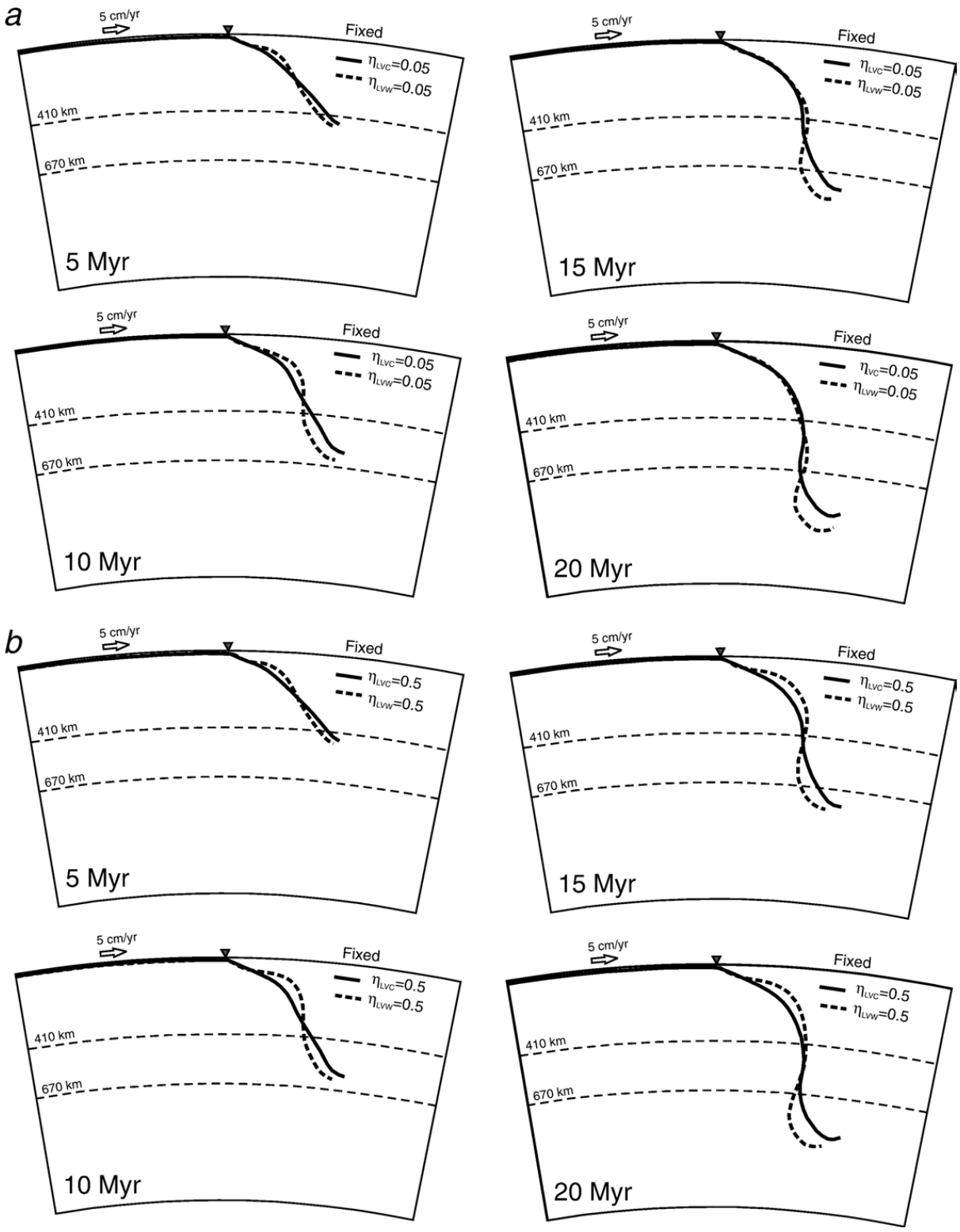

Fig. 8. Comparison of slab shape (trace of subducted oceanic crust) as a function of time for LVW and LVC models. a. Large viscosity reduction ($\eta_{LVW}=\eta_{LVC}=0.05$; $d_{LVC}=30$ km). b. Small viscosity reduction ($\eta_{LVW}=\eta_{LVC}=0.5$; $d_{LVC}=30$ km).

The parameters of the LVC can control the morphology of slabs. Introducing a thin, 30 km LVC on top of the slab, leads to an increased slab dip and a reduced slab thickness (Fig. 7,b,d). Unless there is a LVC down to at least 200 km, slabs continue to become excessively thick. By extending the LVC down to 300 km depth, we are able to decouple the subducting slab from the base of the overriding plate. With such a LVC, slab width within

the upper mantle (<~200 km) approaches the thickness of the oceanic lithosphere before subduction. Extending the LVC deeper than 300 km, we observe a slight slab thickness reduction, but for depths larger than 400 km, there is almost no further slab thinning (Fig. 7a). LVC thickness (d_{LVC}) also controls the slab morphology (as for the cases when η_{LVC} was held constant at 0.1) (Fig. 7b). For a thickness of 10 km (but using a finer 5 km×5 km resolution mesh), the slab still undergoes thickening, but increasing the channel thickness to 20–30 km we observe that the slab thins. A large viscosity drop $\eta_{LVC}=0.01$ in a 10 km thick LVC model does not show significant differences compared with a $\eta_{LVC}=0.1$. There does not appear to be a linear trade-off between LVC viscosity and thickness as the reduction in viscosity more strongly influences slab thickness (and dip) compared to thickness.

For a maximum depth of the LVC of ~100 km, the slab remains at a shallower dip angle at 100–150 km depth. The increase of LVC depth to 400 km gives rise to a slab that changes dip more gradually at 100–150 km depth (Fig. 7c). The same pattern is observed for LVC thickness. Thin channels (~10 km) produce shallow dips at 100–150 km, whereas thick channels generate steeper slabs (Fig. 7d).

When the viscosity reduction is large, the geometry of the LVC or LVW can give rise to similar behavior. We compared the evolution of slab dip for models with LVW ($h_{MAX}=300$ km) and LVC ($h_{MAX}=300$ km, $d_{LVC}=30$ km) for the same viscosity reduction (0.05). Initially (0–10 Myr), the LVW model shows a shallower slab in the upper mantle, but after integrating the models forward for another 10 Myr, the slab dip for both models become similar (Fig. 8a). We also evaluated the evolution of slab dip for models with LVW and LVC for a viscosity reduction of 0.5. The LVW model shows a shallower dipping slab in the upper mantle, which is maintained over 20 Myr (Fig. 8b). Finally, for a channel viscosity of 0.05–1.0, there is no significant difference in slab shape or thickness.

3.3. Volcanic arc evolution

To evaluate the volcanic arc evolution through time and space, we predict the evolution of arc position assuming magma ascent is instantaneous. This assumption is consistent with rapid magma ascent inferred from U–Th isotope disequilibria that suggests transit times from the source of melting to the surface of ~10^3 years (Turner and Hawkesworth, 1997). We track slab position in time at a fixed depth of 100 km and project it to the surface, consistent with the global average of 105 km for the depth of slabs below volcanic arcs (Syracuse and Abers, 2006). From the surface projection, we determine the distance between the estimated volcanic arc and trench (d_{VA}). A LVW changes d_{VA} and can lead to time-dependent values. For example, with $\eta_{LVW}=0.5$, d_{VA} increases linearly for the first 10 Myr then stabilizes at ~320 km (Fig. 9). By decreasing the wedge viscosity by an order of magnitude (to 0.05), we see an increase in the volcanic arc–trench distance in the first 10 Myr of convergence, but then d_{VA} reduces from ~260 km to ~220 km after 20 Myr (Fig. 10a). The maximum depth extent of LVW, can also influence the volcanic arc–trench distance. A deep LVW ($h_{MAX}=400$ km, $\eta_{LVW}=0.1$) produces a volcanic arc that changes position in a similar fashion as a model with a shallow LVW (300 km) but with a greater viscosity reduction (0.05) (Fig. 9b). Also, a shallow LVW ($h_{MAX}=200$ km, $\eta_{LVW}=0.1$) produces a slightly more distant volcanic ($d_{VA}>370$ km) arc compared with the previous model with $h_{MAX}=200$ km and $\eta_{LVW}=0.5$ (Fig. 9b).

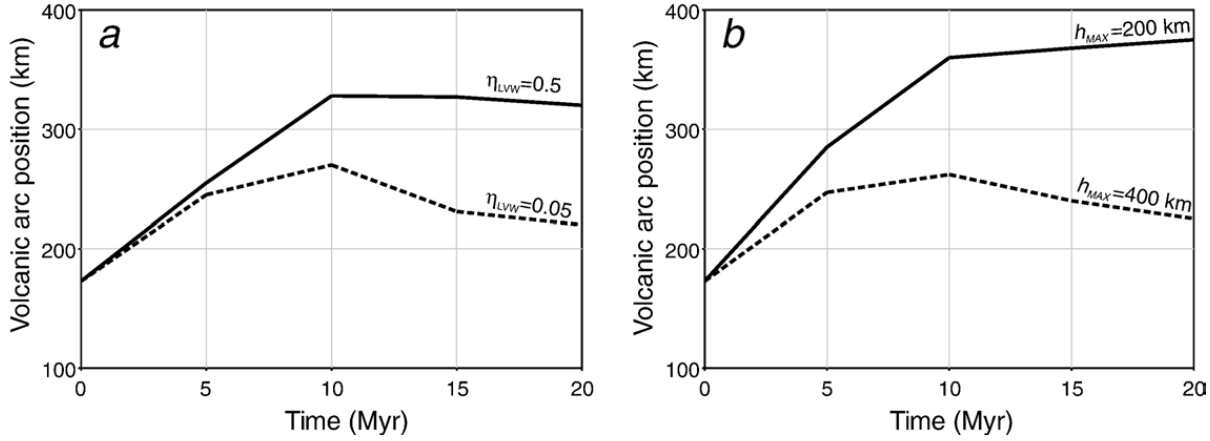

Fig. 9. Predicted volcanic arc position through time for LVW models. Volcanic arc position is defined from the slab at 100 km depth. a. Influence of viscosity reduction in LVZ ($h_{MAX}=300$ km). b. Influence of maximum depth extent of LVW ($\eta_{LVW}=0.1$).

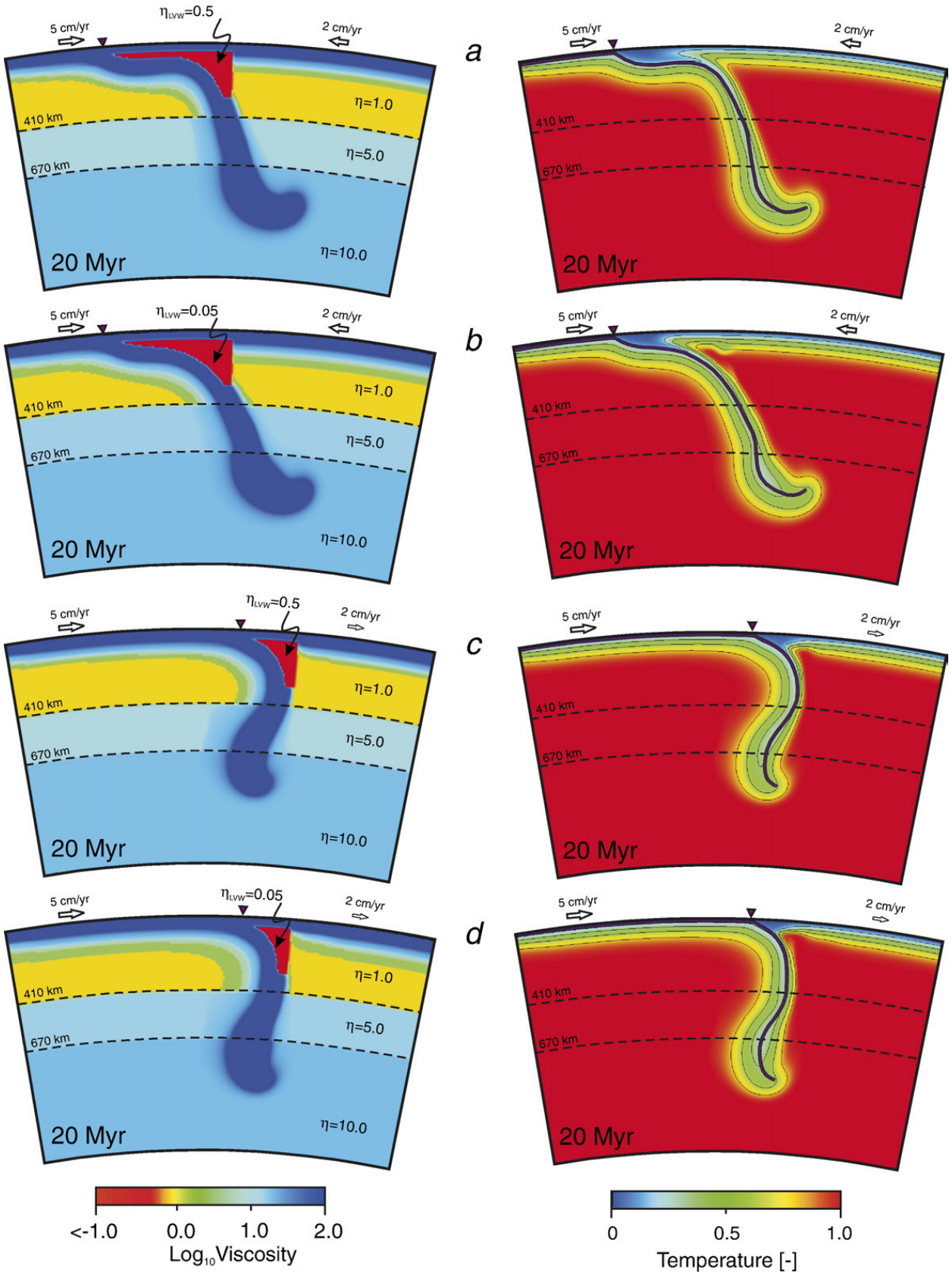

Fig. 10. Trench migration and mantle viscosity reduction influence on subduction zone structure shown through viscosity (left) and temperature (right). a. Rollback model with wedge viscosity reduction of $\eta_{LVW}=0.5$. b. Rollback model with wedge viscosity reduction of $\eta_{LVW}=0.05$. c. Roll forward model with wedge viscosity reduction of $\eta_{LVW}=0.5$. d. Roll forward model with wedge viscosity reduction of $\eta_{LVW}=0.05$.

3.4. Trench rollback with low viscosity wedges and channels

As previously shown (Kincaid and Olson, 1987; Zhong and Gurnis, 1995; Christensen, 1996), trench migration influences subduction zone structure. When all other parameters are held constant, trench migration is positively correlated with increased advective thickening, decreasing slab dips, and the onset of flat-lying subduction. In our models, the rate of trench migration is equal to the overriding plate velocity, and is a constant 2 cm/yr. When we introduce trench rollback, the overall

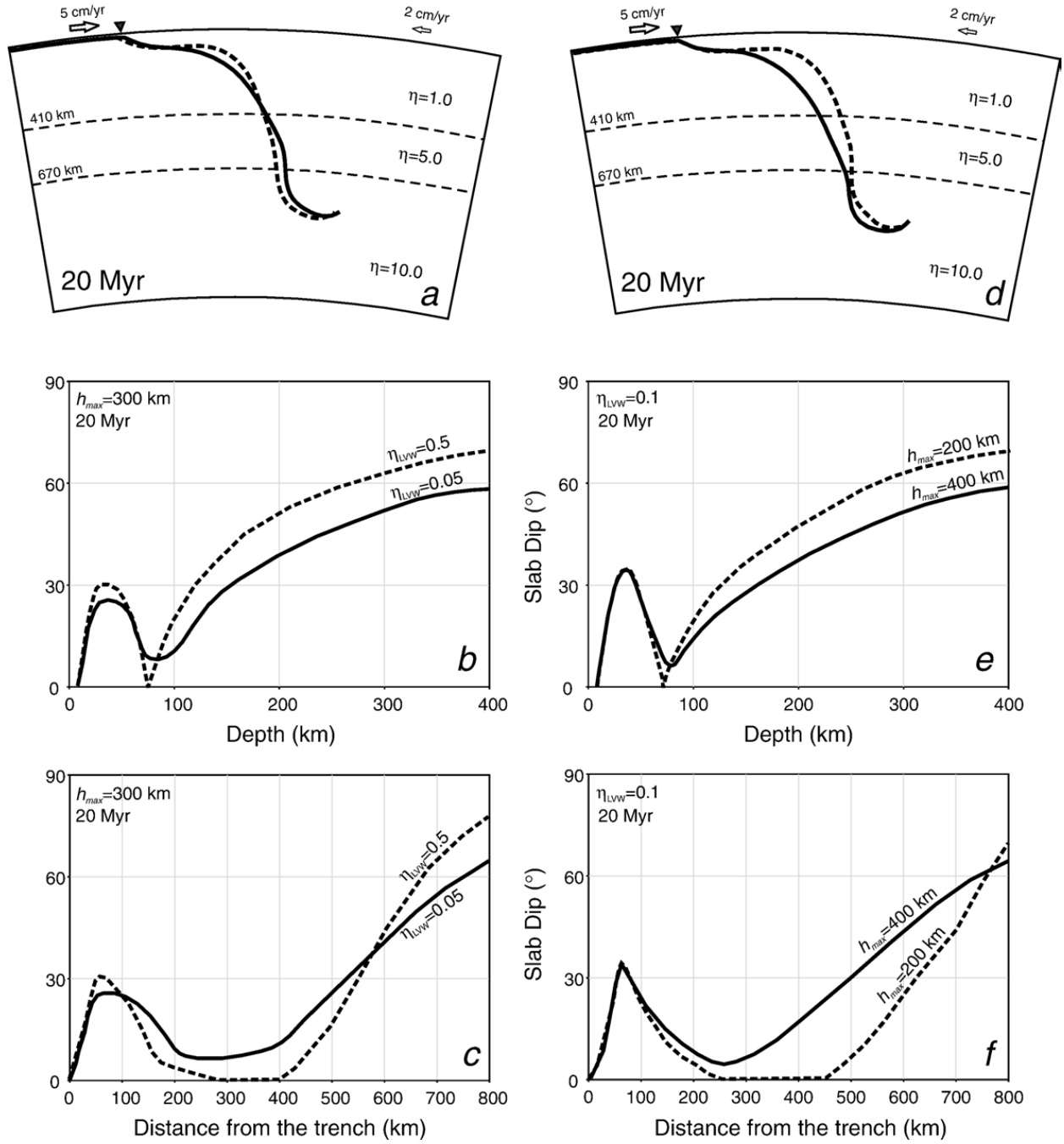

Fig. 11. Local slab dip as function of depth and distance from the trench for models with LVW and trench rollback (v_{OR}=2 cm/yr). a. Comparison of slab shape as a function of time for a large viscosity reduction (η_{LVW}=0.05; η_{LVW}=0.5). b. Slab dip with depth for two models with maximum depth of LVW h_{MAX}=200 and 400 km while η_{LVW}=0.1 is held constant. c. Slab dip for two LVW with η_{LVW}=0.5 and η_{LVW}=0.05 while h_{MAX}=300 km is held constant. a. Comparison of slab shape as a function of time for a maximum LVW depth extension (h_{MAX}=200 km; h_{MAX}=400 km). e. Slab dip variation with distance from the trench as function of maximum depth of LVW (h_{MAX}) while η_{LVW}=0.1 is held constant. f. Slab dip variation with distance from the trench as function of LVW viscosity (η_{LVW}) while h_{MAX}=300 km is held constant.

slab dip decreases when compared with models with a fixed overriding plate (Fig. 10a,b).

On the other hand, introducing trench roll forward (v_{OR}=2 cm/yr), the slab dip increases to almost vertical at the transition zone depth (410 km) (Fig. 10c,d). The mantle viscosity within the wedge was also reduced in these models (h_{MIN}=40 km, h_{MAX}=300 km). The results show that a reduction by a factor of two in the wedge viscosity (η_{LVW}=0.5) produces a perfectly flat slab after 20 Myr (Fig. 11a,c). When the wedge viscosity is decreased further (η_{LVW}=0.05), the slab dip increases (Fig. 11b), even in the presence of trench rollback. The maximum depth of LVW (h_{MAX}) also significantly influences slab geometry. Keeping wedge viscosity constant (η_{LVW}=0.1), while decreasing h_{MAX} from 400 km to 200 km, the slab dip is reduced considerably for depth of 50–100 km. We obtain a flat slab when the maximum depth extent of LVW is reduced to 200 km (Fig. 11d,e,f).

We have shown that in some cases that the presence of low viscosity wedges can promote flat-lying subduction. When combined with trench rollback, the influence of low viscosity can be even more pronounced. A perfectly flat slab was obtained by either reducing the wedge viscosity by half (with respect to the upper mantle viscosity) (Fig. 11a), or by shrinking the vertical extent of the LVW to 200 km depth (Fig. 11d). The onset of the flat slab takes place at 200–250 km from the trench, and the length of the flat-lying portion is 150–200 km (Fig. 11c,f). In some cases, we find that flat-lying subduction can extend nearly 500 km from the trench (Fig. 11f).

In the presence of trench rollback the time-dependence of the slab is included by the presence of a low viscosity channel on top of the slab. While the maximum depth and viscosity reduction (300 km and 0.1, respectively) are kept fixed, we varied the LVC thickness from 10 km to 30 km. With this LVC, the over thickened slab remains attached to the overriding plate and cannot easily sink into the lower mantle (Fig. 12a). Increasing the LVC thickness to 30 km, the slab descends more easily into the lower mantle. In these models, trench rollback can lead to variations in slab dip. It can be seen that the slab dip can be reduced to within ~15° for depths below ~100 km with trench rollback (Fig. 13).

4. Discussion and conclusions

The introduction of low viscosity wedges and channels leads to models of slab structure consistent with that

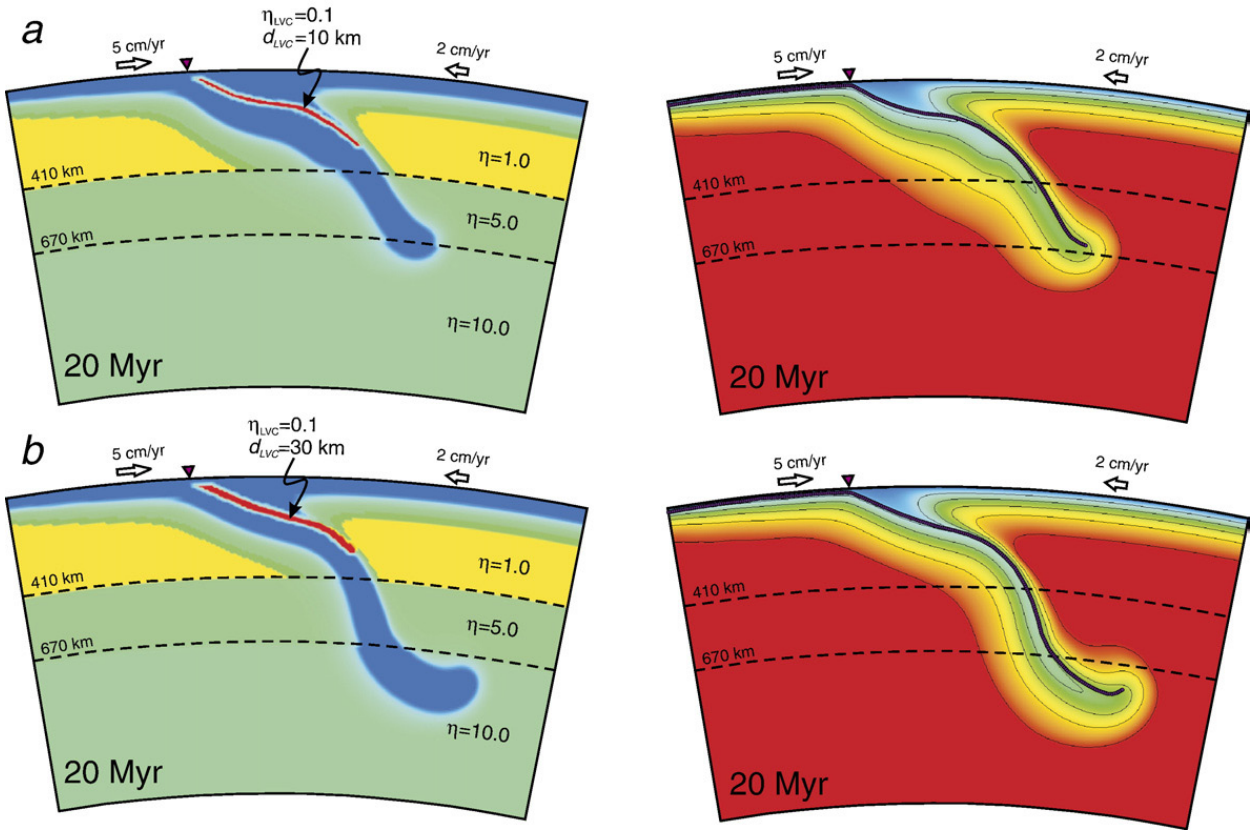

Fig. 12. Viscosity (left) and temperature (right) distribution for models with (a) thin LVC (d_{LVC}=10 km) and (b) thick LVC (d_{LVC}=30 km) and trench rollback (v_{OR}=2 cm/yr).

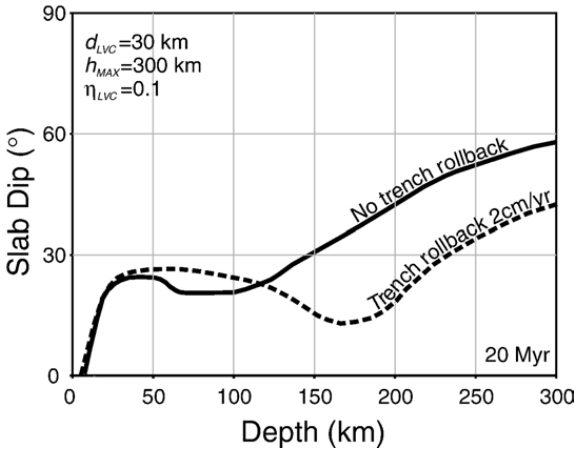

Fig. 13. Local slab dip as function of depth for LVC models (d_{LVC}=30 km, h_{MAX}=300 km, η_{LVC}=0.1) and, with and without trench rollback (v_{OR}=2 cm/yr).

inferred seismically. Previously published partly kinematic models that are similar to the ones here (Christensen, 1996) and fully dynamic models (Zhong and Gurnis, 1995) displayed excessive advective thickening of the slab. Previous attempts to circumvent this problem have utilized techniques in which the overriding plate is removed with a temperature boundary condition set to an isothermal mantle value (Christensen, 1996; Davies, 1999; Tan et al., 2002). Another approach, often used in conjunction with the high-temperature boundary condition, is to impose a large horizontal velocity on the overriding plate in the direction of the subducting plate (e.g., (Christensen, 1996; Tan et al., 2002)) that effectively pushes the slab into the upper mantle. If the purpose of the model is to insert a realistic slab into the deeper mantle, then these boundary conditions are justified. However, if the purpose is to establish a link between the slab and overriding plate or determine controls on slab dip, then these boundary conditions are likely to be inappropriate. The temperature and kinematic boundary conditions are most suited to ocean–ocean subduction with active back-arc spreading and cannot be applied to continental settings especially systems with flat-lying slabs. The new models, although with the mantle wedge viscosity reduction parameterized, provide a more physically realistic mechanism to create subduction.

How the viscosity within the mantle wedge influences slab dip has not been unambiguously established in previous studies. van Hunen et al. (2004) noted that a weak mantle wedge has an influence, but did not quantify the effect. Billen et al. (2003) demonstrated that a low viscosity wedge changes the force balance in subduction zones, but since dip was imposed the relation between wedge viscosity and dip could not be established. However, they found that a good fit to gravity, topography and geoid over the Tonga–Kermadec subduction zone could only be obtained if the viscosity in the mantle wedge was reduced by at least a factor of 10 from the surrounding mantle lithosphere. The introduction of an LVW caused the overriding plate to switch from in-plane compression implying that the suction force on the slab decreased; with a decreased suction force, we expect that slab dip should increase. Arcay et al. (2005) showed that reducing the mantle wedge through slab dehydration caused strong thermal erosion of the overriding lithosphere that develops in less than 15 Myr, and that the location and geometry in the eroded region corresponds to the seismic low-velocity zones observed beneath volcanic arcs. Our models clarify the previous results as both flat-lying subduction or the elimination of flat flying subduction are both permissible outcomes, depending on the geometry of the viscosity reduction. We obtained either steep or flat-slab subduction through variation in two parameters that govern the LVW, the viscosity reduction and its maximum depth. The deeper the LVW and the larger the viscosity reduction, the steeper the slab dip; the shallower the LVW and the smaller the viscosity reduction, the shallower the slab dip.

Volcanism occurs mainly in zones roughly parallel to the trench, while there are some areas where the arc is oblique to the trench, as in Central Mexico. Although the top of the slab below the volcanic arc has generally been found at depths of 90–130 km (Tatsumi, 1986; Tatsumi and Eggins, 1995). Syracuse and Abers (2006) recently showed that slab depth below the volcanic arc correlates moderately with slab dip, but poorly with plate age and convergence rate. In several subduction zones (Central America, South America, Caribbean, Kuril, Tonga–Kermadec), slab dip does not increase steadily with depth. This observation does not favor the slab pull models; rather, it appears that the irregular shape of subduction zones is controlled by other factors in addition to the negative buoyancy and imposed kinematics. Considering the results of (Syracuse and Abers, 2006) in light of our models, suggests that the source regions of arc-volcanism in the wedge might have low effective viscosity. Our models suggest that this tends to increase the dip of slabs locally. This suggests that there is an intimate balance between subduction zone structure, dynamics, and geochemistry/melting behavior. In other words, buoyancy forces do not simply impose a "wedge corner flow" that dehydration and melting then works "within", rather the dehydration and melting may control the slab dip. This would help to explain the poor correlation between tradition geodynamic controls, such as subducting plate age and convergence rates (Cruciani et al., 2005; Tape et al., in preparation).

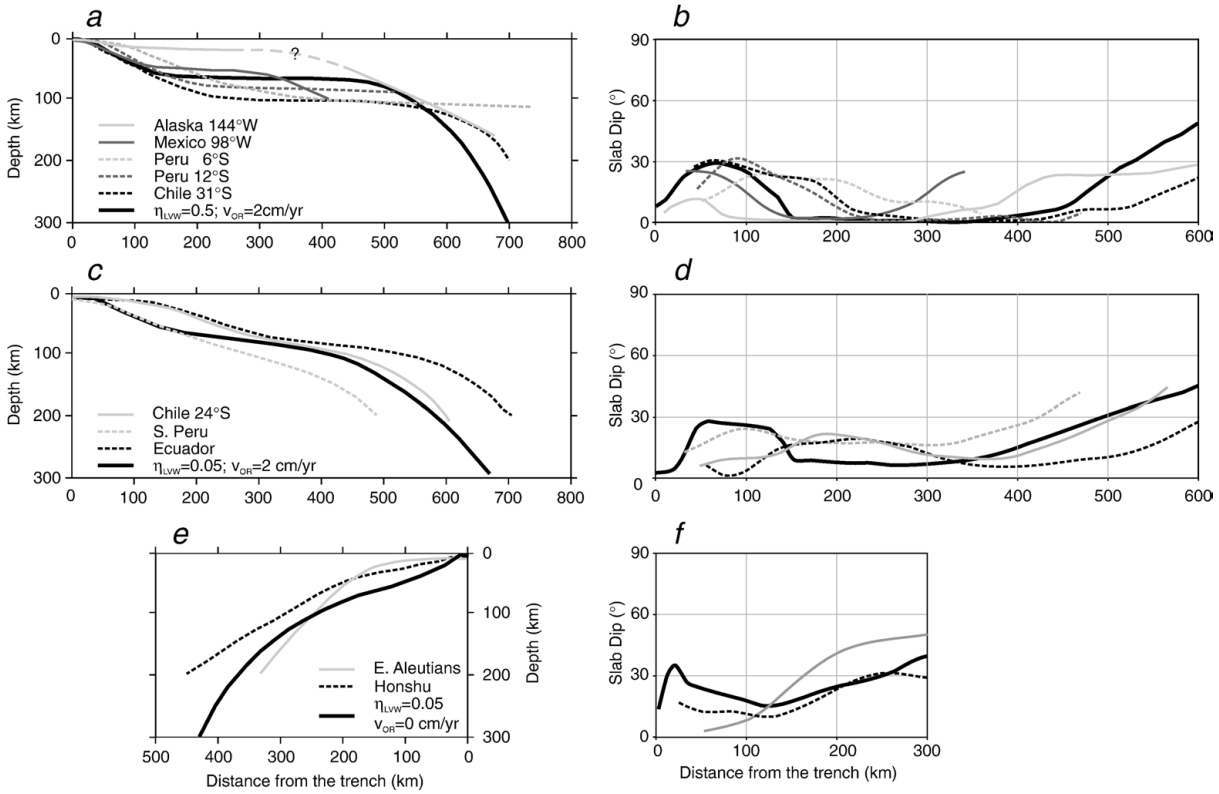

Fig. 14. Slab geometry for various subduction systems (Gutscher et al., 2000; Syracuse and Abers, 2006; Brocher et al., 1994; Ferris et al., 2003) compared with local slab geometry for LVW models integrated over 20 Myr. a. Flat slabs and LVW model ($h_{LVW}=0.5$, $h_{MAX}=300$ km, $h_{MIN}=40$ km, $v_{OR}=2$ cm/yr). b. Slab dip as function of depth and distance from the trench for flat slabs and LVW model. c. Moderately steep slabs and LVW model ($\eta_{LVW}=0.05$, $h_{MAX}=300$ km, $h_{MIN}=40$ km, $v_{OR}=2$ cm/yr). d. Slab dip as function of depth and distance from the trench for moderately steep slabs and LVW model. e. Steep slabs and LVW model ($\eta_{LVW}=0.05$, $h_{MAX}=300$ km, $h_{MIN}=40$ km, $v_{OR}=0$ cm/yr). f. Slab dip as function of depth and distance from the trench for steep slabs and LVW model.

With time-dependent models, we showed that LVWs and LVCs have a significant influence on slab evolution. We show that a LVW with a viscosity an order of magnitude smaller than the upper mantle produces different slab geometries for different LVW maximum depths. It is essential that there must be a localized viscosity reduction for the wedge to influence slab dip. Merely reducing the upper mantle viscosity or thinning the thickness of the overriding plate does not effectively influence slab structure. For example, a shallow LVW (h_{MAX}=200 km) produces a flat-slab structure, whereas extending the LVW down to 400 km, a steeper slab geometry is obtained. The same pattern is obtained by using different viscosity reductions in the mantle wedge above the slab. Introducing only a small reduction in the mantle wedge viscosity (50%), a flat-slab geometry emerged, but reducing the wedge viscosity even more (20 times less than the upper mantle viscosity), moderately steepens the slab. This suggests that if flat-lying subduction is caused by reduced wedge viscosities, then only a narrow range of viscosities will give rise to the phenomena.

Slab geometry for the flat slab in central Chile inferred from hypocenter data (Gutscher et al., 2000) is compared with our LVW model integrated over 20 Myr (η_{LVW}=0.5; h_{MAX}=300 km, h_{MIN}=40 km, v_{OR}=2 cm/yr). The two geometries are similar, although there is a significant difference in the depth of the flat segment (Fig. 14a,b). Other subducted slabs are better fit with our models, for example the slab beneath Peru (12°). The length of the flat slab is consistent although still 10–15 km deeper. The central Mexican slab structure also is similar, even though the length of the flat segment is shorter. The model with a lower mantle wedge viscosity (η_{LVW}=0.05) shows similar slab dip variation with the moderately steep slab beneath Ecuador, although there is a horizontal misfit of ~100 km (Fig. 14c,d). A better match can be seen with the slab beneath Chile for depth below ~100 km. Also, steep slab models (Fig. 5d) fit well the steep slabs beneath Japan (Honshu) and Aleutians (Fig. 14 e,f).

These results suggest that LVW parameters might be inferred from models tailored to individual subduction zones if we use seismic constraints as a proxy for the geometry. For example, a P-wave inversion beneath Tonga arc shows a strong negative velocity anomaly of −6% in the wedge that extends down to ~400 km depth and that extends laterally 50–100 km (Zhao, 2001). This low seismic velocity geometry could serve as a constraint on the present day LVW. Preliminary results from the TUCAN seismic experiment in Central America show a wetter/hotter wedge beneath Nicaragua than beneath Costa Rica (Rychert et al., 2006). This is consistent with our results because the slab dips more steeply beneath Nicaragua than beneath Costa Rica, despite similar plate ages and convergence rates along the trench. Our models have important implications for seismic studies. It is clear that low viscosity wedges or channels may be an important control on slab dip. Consequently, there is a need to refine constraints on the geometry of high seismic attenuation and low seismic velocity regions above slabs. We predict that slab dip should be positively correlated the depth and thickness of the low seismic velocity and high attenuation regions.

The migration of the volcanic arc coupled with magmatic water content could be used to trace the slab and LVW geometry. The models may have implications for the geochemical evolution of volcanic arcs. For example, when volcanic arcs change their distance with respect to distance from the trench, these could be associated with changes in the chemistry of arcs. We predict that there should be a larger volatile input into the wedge when arcs migrate toward the trench and visa-versa. The transition of a subduction zone into the flat flying regime could be preceded by changes in the volatile budget such that there was more dehydration at lower pressures.

Finally, the models may have important implications for the state of stress within the overriding plate when slabs are in the flat-lying regime. We predict that in some cases, there should be efficient decoupling between the slab and overriding plate (Fig. 5d). Some flat-lying subduction systems place the overriding plate into compression. The seismic energy release in the upper plate along the Andes for 250–800 km distance from the trench is 3–5 times larger above the flat slabs than for steep slabs (Gutscher et al., 2000). This would imply a strong coupling between the flat slabs and overriding plate. However, in Central Mexico, there is no evidence for in-plate compression above the flat-lying subduction (Cerca et al., 2004; Cerca et al., 2007; Nieto-Samaniego et al., 2006). It is possible that there are different causes for flat-lying subduction. Gutscher et al. (2000) suggest that the buoyancy of the subducting plate pushes a subduction zone into this regime in which case there may be strong coupling between the slab and overriding plate. The lack of in-plane compression in Central Mexico would suggest the presence of a low viscosity shear zone located above the flat slab.

Acknowledgements

We thank L. Baker, P. Asimow, R. Clayton, D. Helmberger, and M. Chen for discussions. This is contribution number 9159 of the Division of Geological and Planetary Sciences and 55 of the Tectonics Observatory. Principal

support provided through the Caltech Tectonics Observatory by the Gordon and Betty Moore Foundation and supplemented by NSF grants EAR-0205653 and EAR-0609707. All calculations carried out on the Caltech Geosciences Supercomputer Facility partially supported by NSF EAR-0521699.

References

Abers, G., Sarker, G., 1996. Dispersion of regional body waves at 100–150 km depth beneath Alaska: in situ constraints on metamorphism in the subducted crust. Geophys. Res. Lett. 23, 1171–1174.

Abers, G.A., van Keken, P.E., Kneller, E.A., Ferris, A., Stachnik, J.C., 2006. The thermal structure of subduction zones constrained by seismic imaging: implications for slab dehydration and wedge flow. Earth Planet Sci. Lett. 241, 387–397.

Arcay, D., Tric, E., Doin, M.P., 2005. Numerical simulations of subduction zones: effect of slab dehydration on the mantle wedge dynamics. Phys. Earth Planet. Inter. 149, 133–153.

Baker, L., Smith, P., Asimow, P., Gurnis, M., submitted for publication. Emergence of a low-viscosity channel in subduction zones through the coupling of mantle flow and thermodynamic. Earth Planet. Sci. Lett.

Barazangi, M., Isacks, B.L., 1971. Lateral variations of seismic-wave attenuation in the upper mantle above the inclined earthquake zone of the Tonga Island arc: deep anomaly in the upper mantle. J. Geophys. Res. 76, 8493–8516.

Billen, M.I., Gurnis, M., 2001. A low velocity wedge in subduction zones. Earth Planet. Sci. Lett. 193, 227–236.

Billen, M.I., Gurnis, M., 2003. Comparison of dynamic flow models for the Central Aleutian and Tonga–Kermadec subduction zones. Geochem. Geophys. Geosyst. 4 (4), 1035. doi:10.1029/2001GC000295.

Billen, M.I., Gurnis, M., Simons, M., 2003. Multiscale dynamics of the Tonga–Kermadec subduction zone. Geophys. J. Int. 153, 359–388.

Bostock, M.G., Hyndman, R.D., Rondenay, S., Peacock, S.M., 2002. An inverted continental Moho and serpentinization of the forearc mantle. Nature 417, 536–538.

Brocher, T.R., Fuis, G.S., Fisher, M.A., Plafker, G., Moses, M.J., Taber, J.J., Christensen, N.I., 1994. Mapping the megathrust beneath the northern Gulf of Alaska using wide-angle seismic data. J. Geophys. Res. 99, 11663–11685.

Cerca, M., Ferrari, L., Bonini, M., Corti, G., Manetti, P. 2004. The role of crustal heterogeneity in controlling vertical coupling during Laramide shortening and the development of the Caribbean–North America transform boundary in southern Mexico: insights from analogue models. Special Publication of the Geological Society, London. n. 227, 117–140.

Cerca, M., Ferrari, L., López-Martínez, M., Martiny, B., Iriondo, A., 2007. Late Cretaceous Laramide shortening and early Tertiary shearing in the central Sierra Madre del Sur, southern Mexico: insights into the initiation of the Caribbean – North American plate boundary. Tectonics. doi:10.1029/2006TC001981.

Chen, M., Tromp, J., Helmberger, D., Kanamori, H., 2007. Waveform modeling of the slab beneath Japan. J. Geophys. Res. 112, 1–19.

Christensen, U.R., 1996. The influence of plate migration on slab penetration into the lower mantle. Earth Planet. Sci. Lett. 140, 27–39.

Craig, C.H., McKenzie, D.P., 1986. The existence of a thin low viscosity layer beneath the lithosphere. Earth Planet. Sci. Lett. 78, 420–426.

Cruciani, C., Carminati, E., Doglioni, C., 2005. Slab dip vs. lithosphere age: no direct function. Earth Planet. Sci. Lett. 238, 298–310.

Davies, G.F., 1999. Dynamic Earth: Plates Plumes and Mantle Convection. Cambridge Univ. Press.

Ferris, A., Abers, G.A., Christensen, D.H., Veenstra, E., 2003. High resolution image of the subducted Pacific plate beneath central Alaska, 50–150 km depth. Earth Planet. Sci. Lett. 214, 575–588.

Gutscher, M.A., Spakman, W., Bijwaard, H., Engdahl, E.R., 2000. Geodynamics of subduction: seismicity and tomographic constraints from the Andean margin. Tectonics 19, 814–833.

Hasegawa, A., Zhao, D., Hori, S., Yamamoto, A., Horiuchi, S., 1991. Deep structure of the northeastern Japan arc and its relationship to seismic and volcanic activity. Nature 352, 683–689.

Helffrich, G., Abers, G.A., 1996. Slab low-velocity layer in the eastern Aleutian subduction zone. Geophys. J. Int. 130, 640–648.

Hirth, G., Kohlstedt, D.L., 1996. Water in the oceanic upper mantle: implications for rheology, melt extraction and the evolution of the lithosphere. Earth Planet. Sci. Lett. 144.

Hirth, G., Kohlstedt, D.L., 2003. Rheology of the upper mantle and the mantle wedge: a view from the experimentalists. In: Eiler, J. (Ed.), Inside the Subduction Factory Geophysical Monograph, 138. AGU, Washington, DC, pp. 83–105.

Jarrard, R.D., 1986. Relations among subduction parameters. Rev. Geophys. 24, 217–284.

Karato, S., 2003. Mapping water content in the upper mantle, the subduction factory. AGU Monograph, pp. 135–152.

Karato, S., Wu, P., 1993. Rheology of the upper mantle: a synthesis. Science 260, 771–778.

Kincaid, C., Olson, P., 1987. An experimental study of subduction and slab migration. J. Geophys. Res. 92, 13832–13840.

Kohlstedt, D.L., Bai, Q., Wand, Z.C., Mei, S., 2000. In: Bagdassarov, N., Laporte, D., Thompson, A.B. (Eds.), Rheology of partially molten rocks, in Physics and Chemistry of Partially Molten Rocks. Kluwer Academic Roublishers, pp. 3–28.

Lallemand, S., Heuret, A., Boutelier, D., 2005. On the relationships between slab dip, back-arc stress, upper plate absolute motion, and crustal nature in subduction zones. Geochem. Geophys. Geosyst. 6.

Mei, S., Bai, Q., Hiraga, T., Kohlstedt, D.L., 2002. Influence of melt on plastic deformation of olivine–basalt aggregates under hydrous conditions. Earth Planet. Sci. Lett. 201, 491–507.

Nieto-Samaniego, A., Alaniz-alvarez, S., Silva-Romo, G., Eguiza-Castro, M.H., Mendoza-Rosales, C., 2006. Latest Cretaceous to Miocene deformation events in the eastern Sierra Madre del Sur, Mexico, inferred from the geometry and age of major structures. Geol. Soc. Amer. Bull. 118, 238–252. doi:10.1130/B25730.1.

Olbertz, D., 1997. The long-term evolution of subduction zones: a modeling study. Geol. Ultraiectina 149.

Roth, E., Wiens, D., Zhao, D., 2000. An empirical relationship between seismic attenuation and velocity anomalies in the upper mantle. Geophys. Res. Lett. 27, 601–604.

Rychert, C.A., Fischer, K.M., Abers, G.A., Syracuse, E., Protti, M., Gonzalez Salas, V., Strauch, W., 2006. Along-Arc Variations in Attenuation in the Nicaragua–Costa Rica Mantle Wedge. AGU.

Stevenson, D.J., Turner, J.S., 1997. Angle of subduction. Nature 270, 334–336.

Suarez, G., Monfret, T., Wittlinger, G., David, C., 1990. Geometry of subduction and depth of the seismogenic zone in the Guerrero gap, Mexico. Nature 345, 336–338.

Syracuse, Abers, G.A., 2006. Global compilation of variations in slab depth beneath arc volcanoes and implications. Geochem. Geophys. Geosyst. (ISSN: 1525-2027) 7 (5), Q05017. doi:10.1029/2005GC001045.

Tan, E., Gurnis, M., Han, L., 2002. Slabs in the lower mantle and their modulation of plume formation. Geochem. Geophys. Geosyst. 3 (11), 1067. doi:10.1029/2001GC000238.

Tan, E., Choi, E., Thoutireddy, P., Gurnis, M., Aivazis, M., 2006. GeoFramework: coupling multiple models of mantle convection within a computational framework. Geochem. Geophys. Geosyst. 7. doi:10.1029/2005GC001155 Q06001, 14 pp.

Tape, C., Gurnis, M., Kanamori, H., Simons M., in preparation. Subduction zone parameters: observational controls on slab dip and the largest characteristic earthquake. Geochem. Geophys. Geosys.

Tatsumi, Y., 1986. Formation of the volcanic front in subduction zones. Geophys Res. Lett. 13, 717–720.

Tatsumi, Y., Eggins, S., 1995. Subduction zone magmatism. Blacwell Science, Cambridge, MA.

Tovish, A., Schubert, G., Luyendyk, B.P., 1978. Mantle flow pressure and the angle of subduction: non-Newtonian corner flows. J. Geophys. Res. 83, 5892–5898.

Turner, S., Hawkesworth, C., 1997. Constraints on flux rates and mantle dynamics beneath island arcs from Tonga–Kermadec lava geochemistry. Nature 389, 568–573.

van Hunen J., 2001. Shallow and buoyant lithospheric subduction: causes and implications from thermo-chemical numerical modeling, PhD thesis, Geologica Ultraiectina, No. 211, Utrecht University.

van Hunen, J., van den Berg, A.P., Vlaar, N.J., 2004. Various mechanisms to induce shallow flat subduction: a numerical parameter study. Phys. Earth Planet. Inter. 146, 179–194.

Zhao, D., 2001. Seismic structure and origin of hotspots and mantle plumes. Earth Planet. Sci. Lett. 192, 251–265.

Zhong, S., Gurnis, M., 1995. Mantle convection with plates and mobile, faulted plate margins. Science 267, 838–843.